Nucl. Fusion **51** (2011) 094015 (11pp) doi:10.1088/0029-5515/51/9/094015

Overview of FTU results

A.A. Tuccillo[1], L. Amicucci[2], B. Angelini[1], M.L. Apicella[1], G. Apruzzese[1], E. Barbato[1], F. Belli[1], A. Bertocchi[1], A. Biancalani[3,4], A. Bierwage[5], W. Bin[6], L. Boncagni[1], A. Botrugno[1], G. Bracco[1], G. Breyannis[2], S. Briguglio[1], A. Bruschi[6], P. Buratti[1], G. Calabrò[1], A. Cardinali[1], C. Castaldo[1], S. Ceccuzzi[1], C. Centioli[1], R. Cesario[1], I. Chavdarovski[7], L. Chen[8,9], C. Cianfarani[1], S. Cirant[6], R. Coletti[1], F. Crisanti[1], O. D'Arcangelo[6], M. De Angeli[6], R. De Angelis[1], F. De Luca[10], L. Di Matteo[1], C. Di Troia[1], B. Esposito[1], G. Fogaccia[1], D. Frigione[1], V. Fusco[1], L. Gabellieri[1], A. Garavaglia[6], L. Garzotti[11], E. Giovannozzi[1], G. Granucci[6], G. Grossetti[6], G. Grosso[6], Z.O. Guimarães-Filho[12], F. Iannone[1], A. Jacchia[6], H. Kroegler[13], E. Lazzaro[6], M. Lontano[6], G. Maddaluno[1], M. Marinucci[1], D. Marocco[1], G. Mazzitelli[1], C. Mazzotta[1], A. Milovanov[1], F.C. Mirizzi[1], G. Monari[1], A. Moro[6], S. Nowak[6], F.P. Orsitto[1], D. Pacella[1], L. Panaccione[13], M. Panella[1], F. Pegoraro[14], V. Pericoli-Ridolfini[1], S. Podda[1], A. Pizzuto[1], G. Pucella[1], G. Ramogida[1], G. Ravera[1], M. Romanelli[11], A. Romano[1], G. Ramponi[6], C. Sozzi[6], G. Szepesi[15], E. Sternini[1], O. Tudisco[1], E. Vitale[1], G. Vlad[1], V. Zanza[1], M. Zerbini[1], F. Zonca[1], X. Wang[8,9], M. Aquilini[1], P. Cefali[1], E. Di Ferdinando[1], S. Di Giovenale[1], G. Giacomi[1], F. Gravanti[1], A. Grosso[1], V. Mellera[6], M. Mezzacappa[1], V. Muzzini[6], A. Pensa[1], P. Petrolini[1], V. Piergotti[1], B. Raspante[1], G. Rocchi[1], A. Sibio[1], B. Tilia[1], C. Torelli[1], R. Tulli[1], M. Vellucci[1] and D. Zannetti[1]

[1] Associazione Euratom-ENEA sulla Fusione, C.R. ENEA-Frascati, Via E. Fermi 45, 00044 Frascati, Roma, Italy
[2] ENEA Fellow, C.R. ENEA-Frascati, Via E. Fermi 45, 00044 Frascati, Roma, Italy
[3] Max-Planck-Institut für Plasmaphysik, Euratom Association, Boltzmannstraße 2, D-85748 Garching, Germany
[4] Max-Planck-Institut für Sonnensystemforschung, Katlenburg-Lindau, Germany
[5] Japan Atomic Energy Agency, 801-1, Mukouyama, Naka, Ibaraki-ken 311-0193, Japan
[6] Associazione Euratom-ENEA sulla Fusione, IFP-CNR, Via R. Cozzi 53, 20125 Milano, Italy
[7] National Fusion Research Institute, Gwahangno 113, Yuseong-gu, Daejeon 305-333, Korea
[8] Department of Physics and Astronomy, University of California, Irvine, CA 92697-2575, USA
[9] Institute for Fusion Theory and Simulation, Zhejiang University, Hangzhou 310027, People's Republic of China
[10] Dipartimento di Fisica, Università di Milano, via Celoria 16, 20133-Milano, Italy
[11] Euratom-CCFE Association, Culham Science Center, Abingdon, OX143DB, UK
[12] PIIM, Université de Provence, Marseille, France
[13] Associazione Euratom-ENEA sulla Fusione, CREATE, C.R. ENEA-Frascati, Via E. Fermi 45, 00044 Frascati, Roma, Italy
[14] Department of Physics, University of Pisa, 56127 Pisa, Italy
[15] CFSA, University of Warwick, CV47AL, UK

E-mail: angelo.tuccillo@enea.it

Received 8 December 2010, accepted for publication 6 June 2011
Published 31 August 2011
Online at stacks.iop.org/NF/51/094015

Abstract

New FTU ohmic discharges with a liquid lithium limiter at $I_P = 0.7$–0.75 MA, $B_T = 7$ T and $n_{e0} \geqslant 5 \times 10^{20}$ m^{-3} confirm the spontaneous transition to an enhanced confinement regime, 1.3–1.4 times ITER-97-L, when the density peaking factor is above a threshold value of 1.7–1.8. The improved confinement derives from a reduction of electron thermal conductivity (χ_e) as density increases, while ion thermal conductivity (χ_i) remains close to neoclassical values. Linear microstability reveals the importance of lithium in triggering a turbulent inward flux for electrons and deuterium by changing the growth rates and phase of the ion-driven turbulence, while lithium flux is always directed outwards. A particle diffusion coefficient, $D \sim 0.07$ m^2 s^{-1}, and an inward pinch velocity, $V \sim 0.27$ m s^{-1}, in qualitative agreement with Bohm–gyro-Bohm predictions are inferred in pellet fuelled lithized discharges. Radio frequency heated plasmas benefit from cleaner plasmas with edge optimized conditions. Lower hybrid waves penetration and current drive effects are clearly demonstrated at and above ITER densities thanks to a good control of edge parameters obtained by plasma operations with the external poloidal limiter, lithized walls and pellet fuelling. The electron cyclotron (EC) heating system is extensively exploited in FTU for contributing to ITER-relevant issues such as MHD control: sawtooth crash is actively controlled and density limit disruptions are avoided by central and off-axis deposition of 0.3 MW of EC power at 140 GHz. Fourier analysis shows that the density drop and the temperature rise, stimulated by modulated EC power in low collisionality plasmas are synchronous, implying that the heating method is the common cause of both the electron heating and the density drop. Perpendicularly injected electron cyclotron resonance heating is demonstrated to be more efficient than the obliquely injected one, reducing the minimum electric field required at breakdown by a factor of 3. Theoretical activity further develops the model to interpret high-frequency fishbones on FTU and other experiments as well as to characterize beta-induced Alfvén eigenmodes induced by magnetic islands in ohmic discharges. The theoretical framework of the general fishbone-like dispersion relation is used for implementing an extended version of the HMGC hybrid MHD gyrokinetic code. The upgraded version of HMGC will be able to handle fully compressible non-linear gyrokinetic equations and 3D MHD.

(Some figures in this article are in colour only in the electronic version)

1. Introduction

FTU is a circular full metallic tokamak capable of working routinely at ITER magnetic field and plasma density. Moreover its heating systems, 140 GHz-ECRH (electron cyclotron resonance heating) and 8 GHz-LHCD (lower hybrid current drive), provide direct electron heating as in ITER and, because of the machine compactness, high load at wall, allowing significant contribution to ITER-relevant issues. In addition to the full metallic wall, FTU is equipped with a liquid lithium limiter (LLL), whose capability of acting as an effective plasma facing component (PFC) has already been reported [1]. Since the last IAEA-FEC in Geneva, the LLL has been used as a routine tool in FTU, allowing optimal plasma operations thanks to a good control of scrape-off layer (SOL) characteristics. This improvement reflects a widened space of operations with accessible plasma densities well above the Greenwald limit. These high-density discharges exhibit peaked density profiles, good confinement properties [2] and very low plasma contamination with negligible contribution from metallic impurities. Moreover, operations with the LLL allow shaping the density profile to reproduce edge conditions foreseen in the ITER scenario 4 regime, thus allowing a first demonstration of LHCD under ITER conditions [3, 18]. The ECRH system has been widely used for contributing to ITER-relevant issues addressing plasma breakdown optimization, MHD and disruption control and probing plasma transport in the presence of additional heating [4, 5]. The first topic addressed in section 2 of this paper deals with LLL operations. New FTU ohmic discharges at $I_P = 0.7$–0.75 MA, $B_T = 7$ T and $n_{e0} \geqslant 5 \times 10^{20}$ m^{-3} are reported, which confirm the spontaneous transition to an enhanced confinement regime, 1.3–1.4 times ITER-97-L, when the density peaking factor is above a threshold value of 1.7–1.8. A linear microstability analysis reveals the importance of the presence of lithium in the discharge for triggering turbulent inward electron and deuterium fluxes. In this section, the preliminary results of transport analysis of the first pellet fuelled lithized discharges are also reported [2]. In section 3, the results of LH penetration in high-density discharges are reported. A combination of clean plasma, low recycling and high edge temperature, obtained by the LLL and pellet injection, allowed shaping the FTU L-mode plasma density profiles to match those expected in ITER scenario 4: under these conditions lower hybrid (LH) waves penetrated the plasma core demonstrating for the first time a safe path for LH operations in ITER. In section 4, plasma studies with ECRH are reported. Plasma breakdown assisted by ECRH is studied in the framework of a multi-machine effort. Indeed, the pre-formation of a low-density plasma enabling plasma current start-up with a reduced electric field is of utmost relevance for ITER where a low in-vessel toroidal electric field, $E \leqslant 0.3$ V m^{-1}, will be available. In FTU, perpendicularly injected ECRH demonstrated to be more efficient than the obliquely injected one, increasing the range of pressure by about a factor of 4 and reducing the minimum electric field required at breakdown by a factor of 3. The exploitation of ECRH capability in avoiding disruptions at the density limit is also reported in section 4 while the activity in collaboration with the ASDEX Upgrade team can be found in [6]. The results of the control of sawtooth (ST) frequency by modulated ECRH power deposited across the $q = 1$ surface are also reported. ECRH operations in FTU also addressed the issue of particle confinement in the presence of additional heating by probing plasma properties with modulated power. Finally in section 5, the theoretical and experiment modelling activities are reported. The theoretical

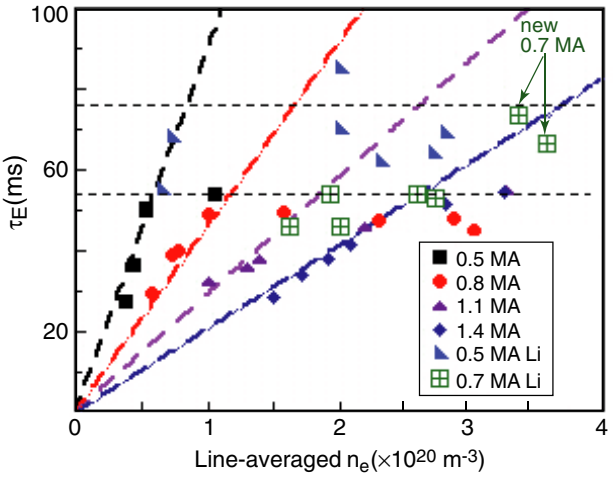

Figure 1. Energy confinement time versus line-averaged density in ohmic FTU 'lithized' discharges.

framework of the general fishbone-like dispersion relation (GFLDR) is applied to construct a solid and systematic interpretative basis for electron fishbone [7] and Alfvénic mode observations in FTU. The GFLDR framework is also used for implementing an extended version of the hybrid MHD gyrokinetic code HMGC [8]. Applications of this eXtended HMGC (XHMGC) code [9, 10] range from FTU electron fishbone to collective excitations of meso-scale Alfvénic fluctuations in FAST [11–13], for which detailed transport analyses have been carried out [14].

2. High-density discharges with LLL

At the last FEC in Geneva, FTU reported on the improvement of plasma operations when using the LLL. In particular, a better energy confinement time, up to $1.4 \cdot \tau_{\mathrm{ITER97-L}}$, was found for the saturated ohmic confinement (SOC) regime with respect to pre-lithium FTU discharges [1]. Lithized discharges always exhibit peaked density profiles, with density as high as 1.6 times Greenwald's value, but the transition to enhanced confinement appears only when the density peaking factor overcomes a threshold value of ∼1.8. The results shown in Geneva were limited to 0.5 MA plasma current, as higher current discharges never reached the peaking threshold. New discharges recently obtained at $I_{\mathrm{P}} = 0.7$ MA, $B_{\mathrm{T}} = 7$ T, $q_{\mathrm{cyl}} \sim 5$, reach densities up to 1.6 times Greenwald's ($\bar{n}_{\mathrm{e}} \geqslant 3.5 \times 10^{20}\,\mathrm{m}^{-3}$) with a peaking factor larger than 2 [2]. These discharges confirm the spontaneous transition to an enhanced value of the confinement time in the SOC regime when the density peaking factor overcomes the threshold value of ∼1.8. In figure 1 a typical value of the confinement time of these discharges is added on the previous database.

Transport analysis with the JETTO code shows that in these discharges the electron thermal conductivity (χ_{e}) decreases as the density increases, while the ion thermal conductivity (χ_{i}) remains close to a typical neoclassical value. A detailed microstability analysis of LLL discharges was carried out with the GKW [15] and GS2 [16] codes to investigate the mechanisms leading to density peaking and improved confinement.

The parameters of FTU shot #30582 (a typical LLL discharge) are reported in table 1 for two selected time slices, at $r/a = 0.6$ (gradient region). During the high-density phase the deuterium and experimental electron fluxes are found to change sign from inwards ($t = 0.3$ s) to outwards ($t = 0.8$ s). Local parameters of table 1 are taken from a semi-interpretative JETTO analysis of shot #30582 which made use of experimental electron temperature and density profiles (Thomson scattering), while ion temperature profiles and Z_{eff} are reconstructed to match the measured neutron yield, radiation, loop voltage and current profile checked against the MHD spectra. This technique was tested for different FTU shots and proved to give a good estimate of the ion temperature profile, q-profile and Z_{eff}. The other relevant parameters in the gradient region are $t = 0.3$ s, $q = 2.76$, $s = 1.62$, $\alpha = 0.1$, $Z_{\mathrm{eff}} = 1.9$, $T_{\mathrm{e}}/T_{\mathrm{i}} = 1.2$; $t = 0.8$ s, $q = 2.36$, $s = 1.5$, $\alpha = 0.25$, $Z_{\mathrm{eff}} = 1.06$, $T_{\mathrm{e}}/T_{\mathrm{i}} = 0.92$. The growth rate of the linearly unstable modes at the two time slices, obtained by a full electromagnetic analysis is reported in figure 2.

The particle fluxes driven by the unstable modes in the same region $r/a = 0.6$ and for the same time slices are shown in figure 3. The different direction of ITG-driven Li flux compared with that of electron and deuterium at $t = 0.3$ s should be noted, while at $t = 0.8$ s all fluxes are in the same direction. To highlight the influence of lithium on driving the electron and deuterium fluxes inwards at the time $t = 0.3$ s, *these fluxes are also computed for the same plasma parameters but without* lithium in the discharge and are plotted for comparison in figure 3(*a*). In the high-density phase, $t = 0.8$ s, Z_{eff} *is nearly one and the fluxes will not change assuming no lithium in the discharge.* The ETG-driven flux is always inwards for all species. As a consequence of the normalization scheme the fluxes shown in the figures are just the initial values of the linear phase of the mode growth rate and carry no information about the saturated flux levels in the non-linear phase. However, their sign does not change and determine the direction of the flux as the mode evolves.

The particle flux (linear) driven by the ETG modes is found to be inwards (negative) for all of the species and at both times. The particle flux driven by the ITG modes is inwards for ions and electrons at $t = 0.3$ s while it is outwards (positive) for lithium. The electron and deuterium fluxes driven by ITG modes change sign at $t = 0.8$ s becoming outwards. By comparing the sign of the linear flux with the particle flux derived from the experimental data (JETTO analysis) it appears that the flux is dominated by short-wavelength ion temperature gradient modes at mid-radius in the gradient region of the discharge. Inside one-third of the minor radius, at $r/a = 0.3$, the ITG modes are found to be stable. The flux at $t = 0.8$ s and $r/a = 0.3$ is driven entirely by ETG modes and is directed inwards for all of the particle species.

The above linear microstability analysis points out the importance of lithium in triggering a turbulent inward flux at mid-radius of the discharge for electrons and deuterium by changing the growth rates and phase of the ion-driven turbulence. The inward flux is sustained in the central region of the discharge through electron gradient dominated transport. The lithium flux in turn is found to be directed outwards at plasma mid-radius that is consistent with the low Z_{eff} value (close to 1.0) as measured during the high-density phase.

Table 1. #30582 plasma parameters at $r/a = 0.6$.

	$t = 0.3$ s				$t = 0.8$ s			
	$\bar{n}_e$ (10^{19})	T (keV)	$-a\nabla T/T$	$-a\nabla n/n$	$\bar{n}_e$ (10^{19})	T (keV)	$-a\nabla T/T$	$-a\nabla n/n$
D^+	3.21	0.47	2.14	0.89	15.50	0.26	4.606	3.118
e^-	6.03	0.57	3.07	0.89	15.95	0.24	4.943	3.118
Li^+	0.94	0.47	2.14	0.89	0.15	0.26	4.606	3.118

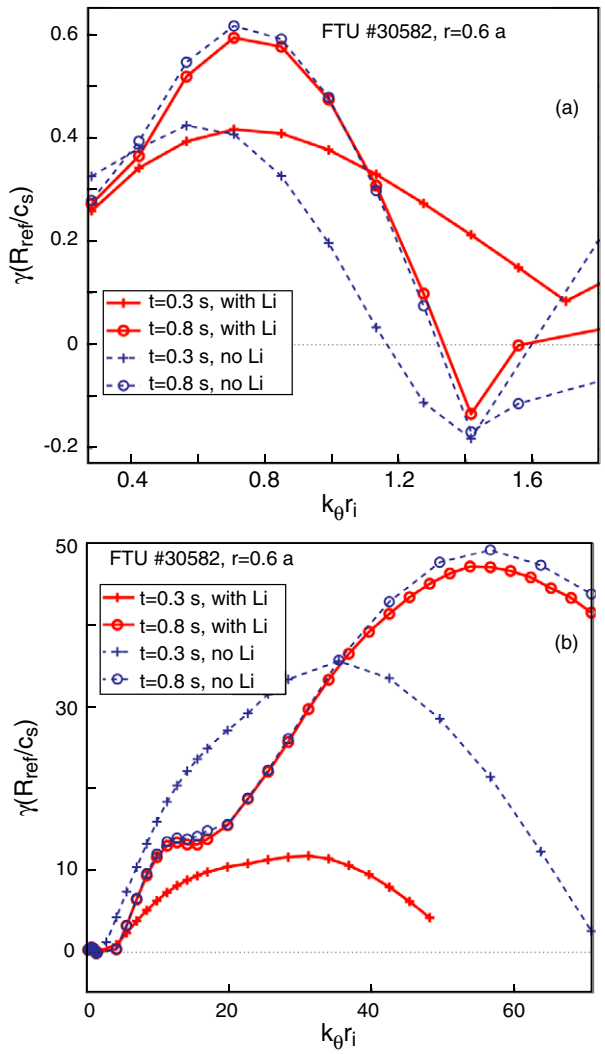

Figure 2. Growth rates of ITG (a) and both ITG plus ETG modes (b) for two time slices $t = 0.3$ s and $t = 0.8$ s at $r = 0.6a$ for FTU shot #30582. Results with the same parameters but without lithium (dashed line). Here $\rho_i = \rho_D$.

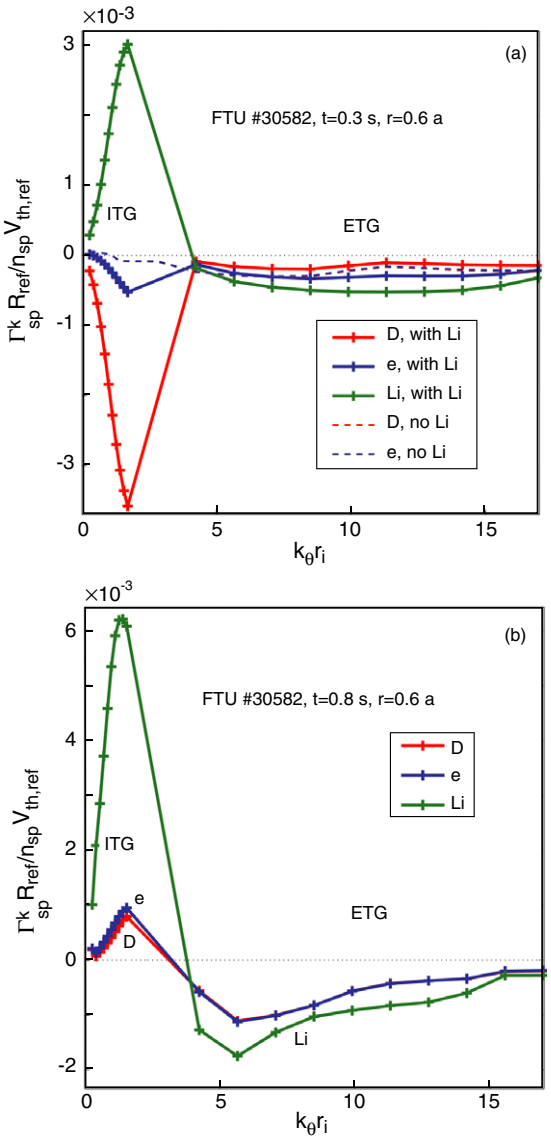

Figure 3. Spectrum of three species particle flux (red: D, blue: e^-, green: Li) driven by $E \times B$ convection of ITG and ETG modes: (a) $t = 0.3$ s, (b) $t = 0.8$ s. Results with the same parameters but without Li are indicated by dashed lines in (a).

High-density discharges were also obtained by the first successful injections of D_2 pellets in the presence of significant wall lithization. Density profiles, for transport analysis, were obtained from the inversion of the FTU CO_2 scanning interferometer [17], which is a very powerful tool for studying fast evolution of density profiles and very strong gradients. Density profiles were taken every 62.5 μs with a spatial resolution of 1 cm and a line integrated density resolution $\Delta\bar{n}_e/\bar{n}_e \approx 2\%$. After a prompt increase in central density, typical of pellet fuelled discharges, a further peaking is observed following the first pellet, which suggests the existence of an inward pinch as seen also in gas fuelled discharges (figures 4 and 5). A fully interpretative transport analysis of the density profile decay (first pellet) was performed in the region where there are no particle sources after the completion of pellet ablation ($r/a < 0.5$). According to particle conservation within each flux surface (S) and under the assumption that the particle flux can be expressed in terms of a diffusive (D) and a pinch term (V), D and V can be determined

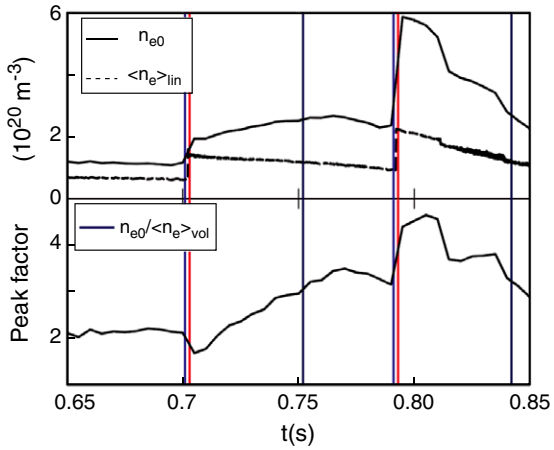

Figure 4. Peak and line-averaged density (top) and density peaking factor (bottom). Vertical lines indicate time slices of profiles shown in figure 5. Blue–red lines distance, which should be only 1 ms, is increased to make them visible. The two blue lines indicate pellet times.

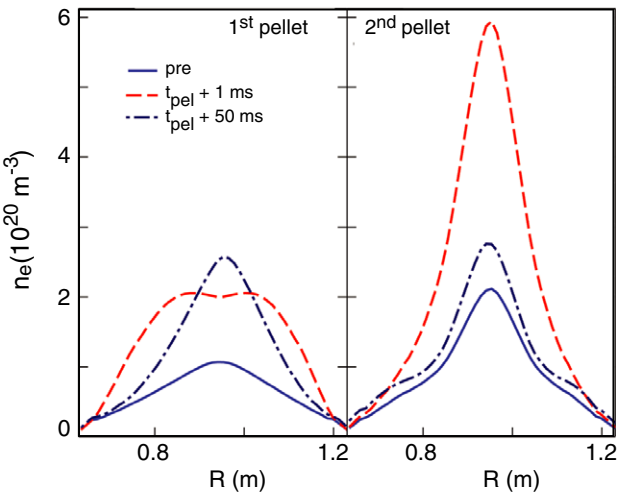

Figure 5. #32552, density profiles in the vicinity of two consecutive pellets.

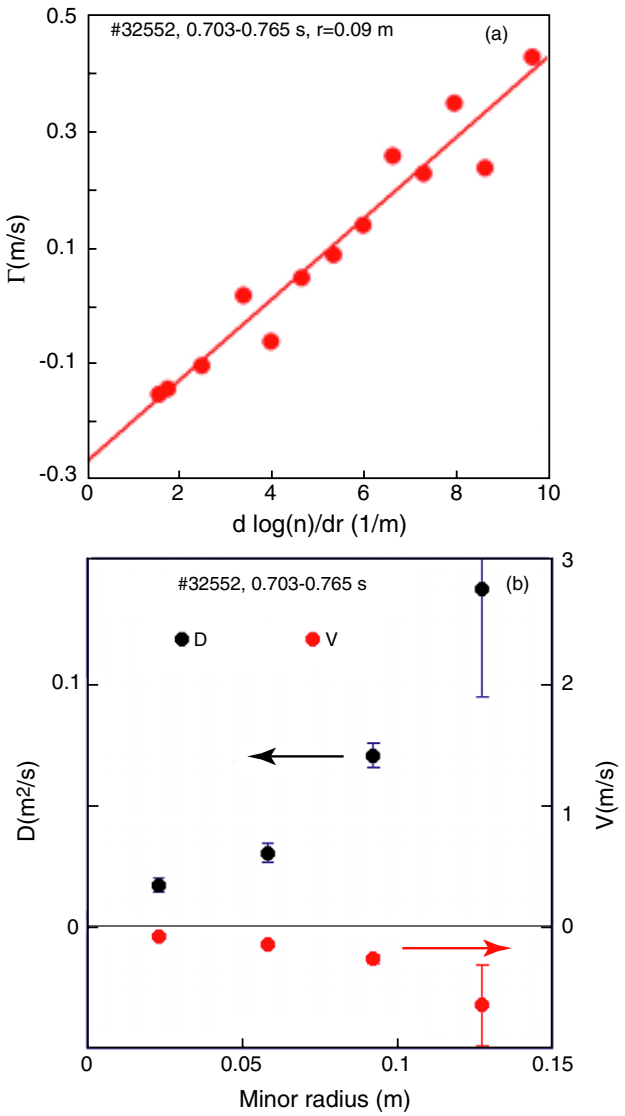

Figure 6. Experimental particle flux at $r = 9$ cm in the post-pellet phase derived from density profiles evolution (a). Diffusion coefficient and pinch velocity versus minor radius (b).

at each radial position from a fit of the experimental data following the pellet transient. Indeed, at each flux surface S, one can plot experimental flux speeds Γ/n (equation (a)) versus the density normalized gradients ($\nabla n/n$) at different times and get, from a linear fit, D and V according to equation (b). Here n is the local density as deduced from the inversion of interferometer data and N is its integration on the volume enclosed in the surface S.

$$(a)\ \Gamma = \frac{1}{S}\frac{\delta N}{\delta t} \qquad (b)\ \frac{\Gamma}{n} = D\frac{\nabla n}{n} + V.$$

Repeating the procedure at different radial positions, D and V profiles are found (figure 6).

This technique gives, at $r/a = 0.3$, a particle diffusion coefficient of $D \sim 0.07\,\mathrm{m^2\,s^{-1}}$ and an inward pinch velocity of $V \sim 0.27\,\mathrm{m\,s^{-1}}$. According to JETTO interpretative simulations, these figures are between neoclassical ($D \sim 0.03\,\mathrm{m^2\,s^{-1}}$; $V \sim 0.14\,\mathrm{m\,s^{-1}}$) and Bohm–gyro-Bohm ($D \sim 0.3\,\mathrm{m^2\,s^{-1}}$; $V \sim 0.5\,\mathrm{m\,s^{-1}}$) values. An analysis of the density decay time in comparison with similar discharges of the pre-lithium phase is in progress and further experiments are planned to produce new non-lithized reference discharges. Finally, pellets have also been used in combination with LH waves for exploring new possibilities of driving plasma current at high densities as described in the following section.

3. LHCD at ITER-relevant density

The LHCD will potentially provide the most efficient tool for actively producing non-inductive current in tokamak plasmas, thus opening a path towards the realization of a steady-state reactor. The occurrence of the LHCD effect, in tokamak plasmas, has been confirmed indeed in many experiments, which, however, operated with densities, in the outer part of plasma column, markedly lower than those required for ITER.

New FTU experimental results have now assessed the plasma conditions enabling the penetration of the coupled

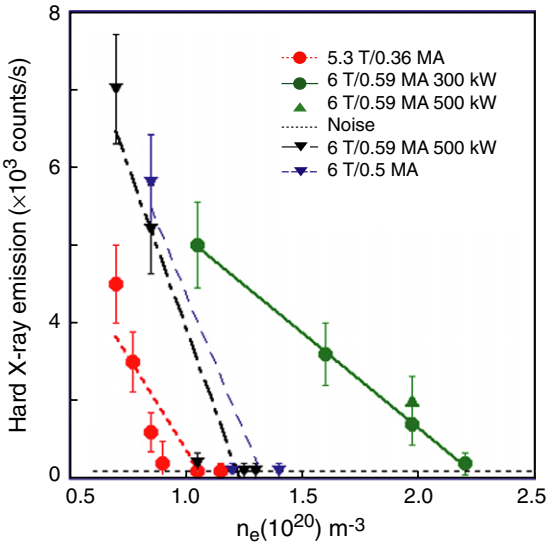

Figure 7. LH-accelerated fast electrons hard x-ray versus plasma density. Unmodified edge (dashed lines) and high T_e edge with lithized wall regimes (full line).

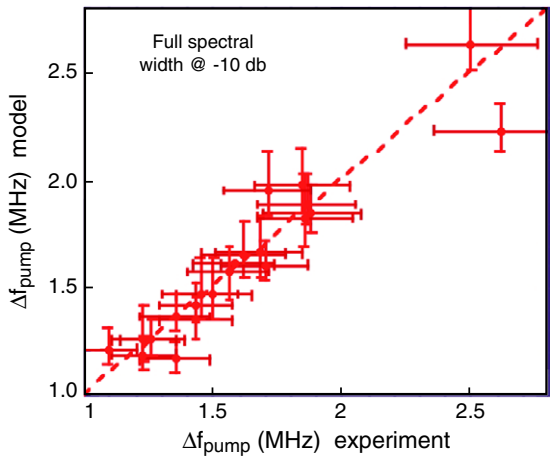

Figure 8. Computed versus experimental LH pump frequency width at −10 dB down the peak.

LH waves' power into the plasma and the consequent LHCD at plasma densities even higher than that required on ITER [3, 18]. Although quasi-linear theory predicts that a properly coupled LH wave would fully propagate into the core of high-density plasmas, recent experiments have shown no penetration or much stronger reduction of driven current than expected with increasing density. This effect already occurs for outer ($r/a \approx 0.8$) density even lower than that expected in ITER [19–21]. In these experiments, the coupled LH power happens indeed to be fully deposited at the very plasma edge when a certain threshold in the plasma density is exceeded. Similar effects are produced by parametric instability (PI) observed in the early LH experiments aimed at plasma core ion heating although other alternative or even concomitant mechanisms can be envisaged. New experiments at very high densities were performed in FTU aimed at modifying the plasma edge conditions, to minimize the PI-produced spectral broadening by increasing the temperature in the outer region of the plasma column [22]. The hard x-ray radiation produced by LH-accelerated supra-thermal electrons was used to monitor the LH penetration and consequent effectiveness in driving current. Figure 7 shows how the hard x-ray emission, recorded along a central line of sight, varies with density. The experimental points connected by dashed lines refer to plasmas with three different sets of plasma currents and magnetic fields with a non-optimized edge: the x-ray emission remains at the noise level for plasma density $\bar{n}_e \geqslant 1.0 \times 10^{20}\,\mathrm{m}^{-3}$ (corresponding to $n_{e0} \approx 1.5 \times 10^{20}\,\mathrm{m}^{-3}$, and $n_{e\_0.8} \approx 0.4 \times 10^{20}\,\mathrm{m}^{-3}$ at $r/a \approx 0.8$). Under these conditions the coupled LH power appears to be fully deposited at the very edge of the plasma. It must be noted that in these discharges the launched LH spectrum, $n_{\|\mathrm{peak}} = 1.9$, is accessible to the plasma centre.

The edge conditions were then modified to produce higher temperatures in the outer part of the plasma column, exploiting lithized wall, proper gas and pellet fuelling [3]. The experimental points connected by the full line in figure 7 refer to these conditions. As evident the LH penetration is recovered at a higher density: $\overline{n_e} \leqslant 2.0 \times 10^{20}\,\mathrm{m}^{-3}$ (corresponding to $n_{e0} \approx 5 \times 10^{20}\,\mathrm{m}^{-3}$, and $n_{e\_0.8} \approx 0.85 \times 10^{20}\,\mathrm{m}^{-3}$ at $r/a \approx 0.8$). As expected by modelling based on PI theory, a reduced spectral broadening is recorded under these conditions, where $T_{e\_0.95} \geqslant 80\,\mathrm{eV}$, despite the very high-density plasmas. The very off-axis electron temperature is obtained by Thomson scattering data and Langmuir probe measurements in the SOL. A width of about 7 MHz was indeed measured at 35 dB below the pump power peak, against 15 MHz measured in lower density plasmas with unmodified edge conditions, where $T_{e\_0.95} \leqslant 50\,\mathrm{eV}$.

For the sake of completeness the same data are also compared with a linear model accounting for LH wave diffusion by density fluctuations in the SOL [23, 24]. Experimental spectral broadening, 10 dB down the peak, is extremely well reproduced by this model, as shown in figure 8, although the sidebands of the experimental spectrum (>20 dB down the peak) appear broader, suggesting additional acting mechanisms. Only a detailed measurement of plasma periphery parameters and their gradients will allow discriminating between the relative weights of the different phenomena in preventing LH wave penetration. However, FTU experiments have shown that, by controlling edge conditions, LHCD experiments can safely be designed for ITER scenario 4, where the high expected edge temperature will exclude any degradation of LH wave penetration in the full range of plasma densities relevant for a thermonuclear reactor plant.

4. ECRH studies

Experiments based on the exploitation of ECRH power were carried out on FTU addressing ITER-relevant issues, such as control techniques (ST and disruptions), plasma formation (breakdown and start-up) and plasma probing for transport studies.

ST control is a critical issue for plasma confinement [25], as large crashes can destabilize NTMs degrading plasma performance, on the other hand ST activity is useful in burning plasma to prevent ash accumulation in the plasma core.

ST destabilization, already performed on FTU by non-modulated ECCD [26], has been further investigated recently,

using 500 ms of repetitive short pulses from two gyrotrons (0.770 MW), inducing the crash either by ECH and co-ECCD. This highly localized power is capable of locally modifying the plasma current density changing the resistivity and the magnetic shear, thus acting on the ST period. A ramped toroidal field $B_T = 5.3$–5.9 T allowed pushing the EC absorption radius r_{abs} inside the ST inversion radius r_{inv} ($q = 1$) up to $r_{abs} \sim r_{inv}/2$, to find the B_T value corresponding to ST crash induced by the EC trigger. Figure 9(*a*) shows the effect of the ECH inside the inversion radius on the ST crash for $B_T = 5.44$ T. The ST destabilization, when ECH is localized inside the inversion radius, is indicated by the reduction of the ST period, with respect to the ohmic one, from ~6 to 2–4 ms, as shown by the time delays between the EC power on/off and the first corresponding crash, figure 9(*a*). Very different behaviour is found at $B_T = 5.51$ T where the ECH deposition is just on the inversion radius, as shown in figure 9(*b*). Here the ST is stabilized when the EC power is on: time delay of the crash ~8 ms, i.e. larger than the ohmic period, while ST is destabilized when the EC power is switched off: crash delay ~3 ms. Figure 9(*c*) shows the combined effects on time delay of ECH + coECCD during the field ramping: the ST period is still shortened at the on/off switching of the EC power, crash delay ~3–4 ms, when EC deposition is inside the inversion radius up to $t = 0.72$ s, while is lengthened when the EC absorption moves outside the $q = 1$ surface, crash delay ~8–10 ms. In this case ST destabilization is obtained when the EC power is turned off, crash delay $\leqslant$6 ms. The next experimental campaign will aim at controlling the ST period at a specific chosen value.

Disruption avoidance by ECRH was demonstrated in previous FTU experiments with off-axis ECRH in disruptions induced by Mo injection [1, 27, 28] and with on-axis ECRH in density limit disruptions [29]. Similar results were obtained in ASDEX Upgrade in density limit disruptions with off-axis ECRH [29]. The technique is based on the stabilization of MHD modes through localized deposition of ECRH on a resonant surface. In recent density limit experiments in FTU, disruption avoidance has also been achieved by injecting off-axis ECRH power (P_{ECRH}). The loop voltage is used as a disruption precursor signal for ECRH real-time triggering. P_{ECRH} (140 GHz, $B_T = 5.3$ T) is deposited at an off-axis location ($r_{dep} \sim 14$ cm) compatible with the $q = 2$ surface ($r_{q=2} = 13 \pm 1$ cm): figure 10 shows the results for two discharges with different levels of P_{ECRH}. Note that, due to the lithium-conditioned walls, the Greenwald limit ($\sim 1.4 \times 10^{19}$ m^{-3}) is largely exceeded in these discharges. The role of ECRH is not to replace the power lost by the plasma, but to provide stabilization of the MHD mode that leads to the disruption. The disruption occurs, as in the reference case (red curve), when the power is halved (black curve) or deposited very far from a rational surface (not shown). Taking into account that the fraction of absorbed power, computed by the quasi-optical ray-tracing code ECWGB 3D [30], is ~40% (corresponding to 0.34 MW in discharge 32081 and 0.19 MW in discharge 32086), we can estimate $P_{ECRH} = 0.27 \pm 0.1$ MW as the average value of ECRH power to be absorbed in the $q = 2$ surface for disruption avoidance in these FTU discharges at $I_p = 350$ kA.

Probing of FTU L-mode ohmic discharges by modulated ECH shows that the central density drop and the resulting

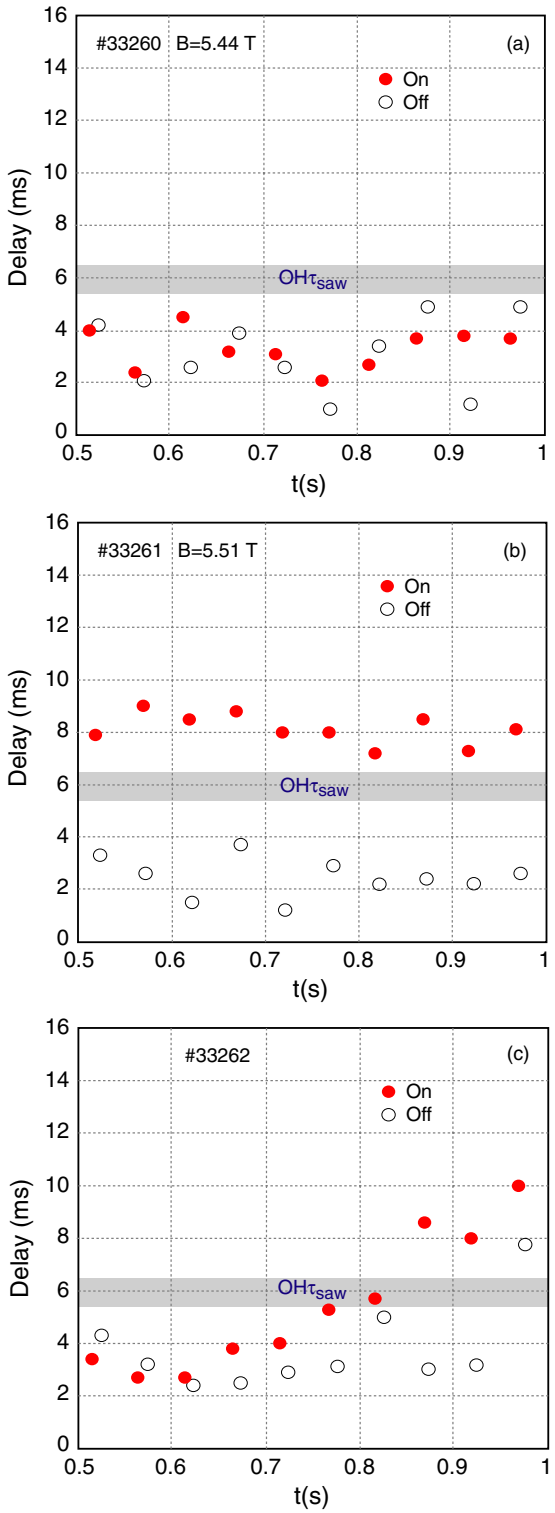

Figure 9. Time delay of ST crash with respect to ECRH power switch on–off. ON, t_{ON}–t_{CRASH} (red filled dots), and OFF, $t_{OFF} - t_{CRASH}$ (black open dots), for $P_{ECRH} = 0.77$ MW, modulated: 10 ms on and 40 ms off. The shadowed area indicates the ohmic period for the investigated discharges. Only in (*a*) ECRH power is deposited inside the $q = 1$ surface (ST destabilization). In (*b*) ECRH power is deposited just at the $q = 1$ surface (ST stabilization at EC ON and destabilization at EC OFF). In (*c*) a combination of ECRH and ECCD is used while the magnetic field is ramped up so that deposition moves from inside to outside the $q = 1$ surface, all of the trends found in (*a*) and (*b*) are recovered.

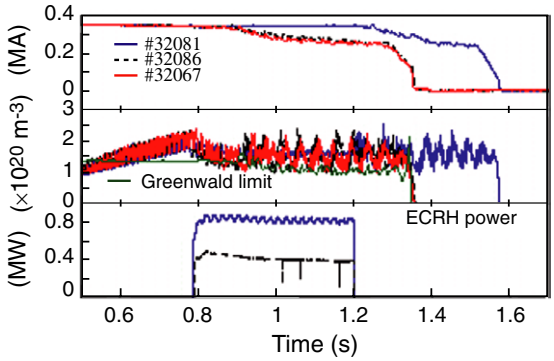

Figure 10. Time traces, from top, of I_P, $\bar{n}_e$ and P_{ECRH} in the reference density limit disruption (#32067) and in two discharges with off-axis ECRH (#32081, $P_{ECRH} \sim 0.8$ MW; #32086, $P_{ECRH} \sim 0.4$ MW).

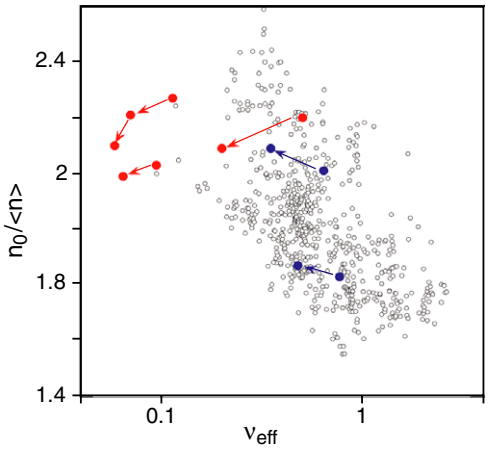

Figure 11. Density peaking versus ν_{eff} in OH FTU discharges ($B_T = 6$ T, $I_P = 0.55$ MA) (open grey symbols), EC heated discharges (red and blue dots). Arrows point from the OH to RF heated phase.

flattening of the density profile are not a by-product of plasma heating. Indeed, Fourier analysis of density and temperature time traces clearly shows that the density drop and the temperature rise in low collisionality plasmas are synchronous.

This implies that the RF heating method is the common cause of both the electron heating and density drop. The lack of delay between the time evolution of the density and temperature excludes that T_e or the ratio T_e/T_i could be the cause of the flattening of the n_e profile. The generation of an energetic tail in the electron distribution function sustained by RF injection probably determines the spatial diffusion of the energetic electrons [31].

This would suggest that collisions, rather than density or T_e/T_i, are the key parameter of the density profile response to the ECH heating. Indeed we observe in figure 11 that, in FTU discharges with effective collisionality $\nu_{eff} \propto (z_{eff}\langle n\rangle R/\langle T_e\rangle^2) < 1$, the density profile peaking, $n_0/\langle n\rangle$, which in general increases by decreasing ν_{eff} [32, 33], decreases with the ECRH power injection. When ν_{eff} is close to 1, in contrast, the density peaking recovers its ohmic behaviour and the ECH power, by increasing T_e, reduces ν_{eff} and builds more peaked density profiles.

Experiments on ECRH-assisted breakdown were carried out on FTU, contributing to the multi-machine effort aiming at defining the optimum start-up scenarios for ITER [4, 5]. Injecting up to 800 kW of EC power in O mode, the FTU plasma start-up pressure is increased by a factor 4 with respect to ohmic values, while a minimum electric field of 0.4 V m^{-1} at the breakdown is obtained for perpendicular EC injection (0°). A reduced efficiency is found for oblique injection (20°), which exhibits a lower plasma current ramp-up rate and higher power to overcome the radiation barrier: a factor 2 higher power is needed to obtain the same results. This is probably connected with a positive effect of wall reflection in the case of 0° injection that locally enhances the power. Indeed, in FTU the circular cross section of the inner limiter surface, in front of the launcher, produces a focalization in the region of resonance, where constructive interference between the backward and forward waves takes place. Therefore, crossing the resonance layer, electrons can be accelerated (when they are in the positive interference region) by a strong wave electric field (up to four times assuming equal intensity for the two waves) gaining enough energy to sustain ionization. On the other hand, a 20° angle shows a better performance in generating a pre-ionized plasma, with higher and wider electron density profiles. This is probably related to a different absorption mechanism of the XM polarization generated, for obliquely propagating wave, after the first reflection from the wall. The EC-assisted breakdown is also devoted to reduce ohmic flux consumption. With off-axis EC resonances a faster current ramp-up is obtained with a reduction of 16% with respect to the central resonance position when a modest flux saving (6%) is due to the resistivity variation, a consequence of higher T_e with ECRH. Changing toroidal field the resonance is moved, inner or outer, at $\sim 0.5r/a$; a faster current ramp-up is obtained in both cases, with a further reduction of 16% in flux consumption with respect to the central resonance case. A strong reduction (factor 3) of plasma internal inductance during the current ramp-up phase is calculated from experimental pressure and equilibrium code reconstruction. This is in agreement with the observed faster current rise, even if more experiments are required to confirm the relationship between ECRH preionization and internal inductance reduction.

5. Theory and modelling of experimental observations

The theoretical framework of the GFLDR was applied to interpret evidence of high-frequency fishbone at JET [34, 35] and to construct a solid and systematic interpretative basis for electron fishbone [7] and Alfvénic mode observations in FTU.

A model based on overdriving a dynamic system near self-organized criticality is proposed for qualitatively explaining (electron) fishbone bursting behaviour [36], which is observed with sufficiently strong perpendicular and parallel supra-thermal electron populations, generated by LHCD power and modelled by a quasi-linear ray-tracing code [37, 38]. Experimental proofs, meanwhile, are provided by various tools: magnetic coils, soft x-ray, hard x-ray, ECE and by interpretative simulations with the JETTO transport code, constrained by magnetic reconstruction measurements. FTU experimental observations have provided the first evidence of strongly non-linear behaviour in connection with electron fishbone excitations by LH only [34] and show clear evidence

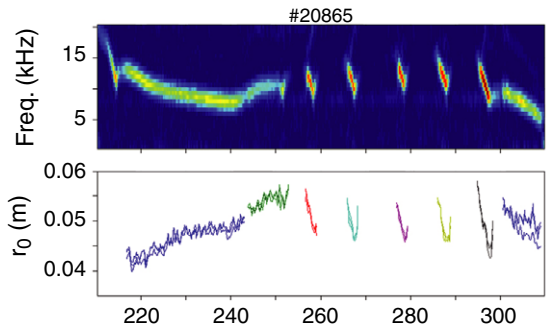

Figure 12. Spectrogram of the electron temperature oscillations (top) and radial position (bottom) of the induced T_e oscillations due to e-fishbones in FTU #20865.

of fast electron redistributions [7]. These results suggest that the level of LH power input controls the transition from nearly steady-state non-linear oscillations (fixed point) to bursting electron fishbone oscillations (limit cycle) and that, in the bursting regime, the fishbone is an energetic particle mode (EPM) [39] well above marginal stability and associated with significant fast electron redistributions, analogous to the fast ion losses that are expected when ion fishbones are excited. Recently, a new ECE analysis technique [40] has been applied to study the mode localization for electron fishbone modes in both almost-stationary and bursting regimes. Figure 12 shows that the e-fishbone-induced T_e oscillations slowly drift outwards in the almost-stationary regime, while they rapidly drift inwards in the bursting regime. The 'fixed point' mode seems to be saturating when the supra-thermal particle scattering out of the resonant region is continuously balanced by the source. Bursting appears with stronger drive, which pushes the system away from marginal stability and causes strong particle redistributions, slowly restored by sources. In other words, the strong regime is far from all descriptions based on proximity to marginal stability, which clearly do not apply at sufficiently strong drive, as shown in the original works on fishbones [41, 42] and confirmed more recently [43, 44]. More recently, FTU experiments studied fishbone-like modes with a slightly reversed q-profile approaching the condition $q_{\min} \approx 1$ and a marginally over-critical population of fast electrons produced by LH, aimed at exploring the critical threshold for mode destabilization [7]. New experiments are in progress in FTU to fully assess the electron fishbone phenomenology by a higher LH power and different LH power waveforms, necessary for destabilizing modes at $q_{\min} \geqslant 2$. Experiments are designed for producing higher supra-thermal electron tail temperatures via ECRH–LH synergy, yielding high pressure gradients for effective excitation of electron fishbone in the high-frequency range. The need of coupling LH power in the early phase of plasma current ramp-up, to match the desired $q_{\min}$, makes the experiment quite difficult. So far, it has been possible to couple the available LH power in the range 0.3–0.6 MW during the plasma current ramp-up, by adopting a change in the FTU switching circuit and using the new favourable operation conditions provided by the lithizated vessel facility. The next experiments will be aimed at increasing the LH power (above 0.8 MW), in order to have an effective LH–ECRH synergy.

Beta-induced Alfvén eigenmodes (BAE) have been observed in DIII-D with strong neutral beam heating [45], during tearing mode in FTU and TEXTOR ohmic plasma [46, 47] and more recently with ICRH during a ST cycle in ASDEX Upgrade [48] and Tore Supra [49], as well as in both ohmic and ECRH plasmas in HL-2A [50], in connection with supra thermal electrons. BAE phenomena are generally very important to the understanding of dynamic behaviour of collisionless plasmas of fusion interest, for they occur in the low-frequency kinetic thermal ion (KTI) gap [51] in the shear Alfvén wave (SAW) continuous spectrum, where various processes characterize the complex behaviour of burning plasmas on long time scales [51–53]. The GFLDR framework [39, 42, 54, 55], usually employed for discussing circulating thermal plasma particle kinetic compression effects on low-frequency SAW [56], was adopted to discuss trapped thermal particle effects on the structures of the low-frequency shear Alfvén continuous spectrum [57], emphasizing their crucial roles in interpreting experimental observations [58, 59]. Recently, we also carefully reconsidered some long (>200 ms) BAE observed in FTU [60]. As observed previously [46, 61] these are oscillations at frequencies between 30 and 50 kHz, accompanying tearing modes with frequencies below 10 kHz and with intensities two order of magnitude less than the tearing modes. BAE frequency scales mainly with the sound speed, and does not scale exactly with the Alfvén frequency [46]. They are characterized by two main frequency lines, which merge into a single line when the island oscillation frequency becomes very low. Mode analysis indicated poloidal and toroidal mode numbers $|m| = 2$, $|n| = 1$. The BAE frequency lines have $|n| = 1$, the higher ones propagating in the same direction with respect to the island, while the lower lines propagate in the opposite direction. The difference between the two BAE frequency lines is exactly twice the fundamental frequency of the tearing mode. The frequency difference can be explained as a Doppler shift due to island rotation, so that BAE forms a standing wave composed of two waves propagating with opposite velocities in the island rest frame. A similar phenomenology was also observed in TEXTOR [47] and in HL-2A [50]. The spectrum obtained by the bicoherence analysis of magnetic coil signals shows that the BAE and tearing oscillations always start with the same phase, thus, it confirms the strong coupling between the two modes when the magnetic island is not locked. The observed BAE frequency in FTU is in agreement with theoretical predictions [61–63], with the observed frequency just below the predicted BAE SAW continuum accumulation point and strong correlation between BAE and tearing mode. We observe that, during the first part of island growth, the BAE frequency increases roughly linearly, in good agreement with theoretical prediction (solid line in figure 13); on the other hand a discrepancy is found for $\delta B_r(r_s)/B_\vartheta(r_s) > 10^{-3}$, where BAE frequency remains rather constant. Therefore, we can confirm that perturbative theory predictions [62, 63] give consistent results only for low magnetic island amplitudes.

The GFLDR framework has also been used for implementing an extended version of the hybrid MHD gyrokinetic code HMGC [8, 64], which simultaneously handles two generic initial particle distribution functions in the space of particle constants of motion. Applications of

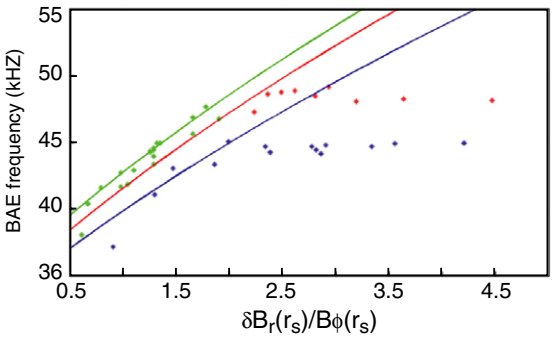

Figure 13. Observed and computed BAE frequency as a function of island width ($\delta B_r(r_s)/B_\vartheta(r_s) > 10^{-3}$) for FTU shots 23184 (green), 25877 (blue) and 26644 (red).

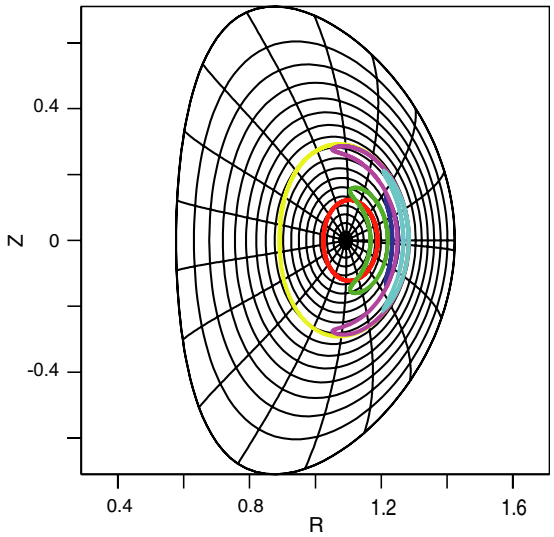

Figure 14. Energetic particle orbits in a ITER-like equilibrium configuration, produced by the new hybrid MHD gyrokinetic code HYMAGYC. Different colours refer to orbits of particles with different $V_{\text{perpendicular}}$ to V_{parallel} ratio, in particular yellow and red orbits refer to passing particles, other colours to trapped particles; extreme combination of parameters is used to check numerical robustness.

this eXtended HMGC (XHMGC) code [9, 10] range from FTU electron fishbone to collective excitations of meso-scale Alfvénic fluctuations in FAST [11], for which detailed transport analyses have been carried out [14]. These investigations assume FAST equilibrium profiles as initial conditions, after the self-consistent dynamic formation of the FAST scenarios is obtained iteratively by interfacing several numerical tools: transport codes (JETTO and the CRONOS suite of codes, including NEMO and SPOT) and the ion cyclotron resonance heating (ICRH) full wave code TORIC, coupled with the quasi-linear solver SSFPQL, which accounts for both ICRH and negative neutral beam injection (NNBI) [14]. Before its use as a numerical investigation tool for supra-thermal particle physics, the XHMGC code has been verified against analytic theories [65] as well as global gyrokinetic codes, such as GTC, in common validity parameter regimes [66].

Strong efforts have focused on completing the implementation of the upgraded version of HMGC [8, 64] to handle fully compressible non-linear gyrokinetic equations and 3D MHD [67, 68]. The new code HYMAGYC (HYbrid MAgnetohydrodynamics GYrokinetic Code) is built by interfacing a modified version of the CHEASE code [69] (equilibrium), an initial-value version of the original eigenvalue MHD stability code MARS [70] (field solver) and an originally developed gyrokinetic particle-in-cell module, yielding the energetic ion pressure tensor needed to close the MHD equations. Figure 14 shows the typical energetic particle orbits in an ITER-like equilibrium configuration, produced by the new code HYMAGYC.

References

References presented below as papers at this conference are available online at http://www-naweb.iaea.org/napc/physics/FEC/FEC2010/html/index.htm

[1] Tuccillo A.A. *et al* 2009 *Nucl. Fusion* **49** 104013
[2] Mazzitelli G. *et al* 2011 *Nucl. Fusion* **51** 073006
[3] Cesario R. *et al* Lower hybrid current drive at densities required for thermonuclear reactors, EXW/P7-02
[4] Granucci G. *et al* 2011 *Nucl. Fusion* **51** 073042
[5] Stoeber J. *et al* 2011 ECRH assisted plasma start-up with toroidally inclined launch: multi-machine comparison and perspectives for ITER *Nucl. Fusion* submitted
[6] Esposito B. *et al* 2011 Avoidance of disruptions at high β_N in ASDEX Upgrade with off-axis ECRH *Nucl. Fusion* submitted
[7] Cesario R. *et al* 2009 *Nucl. Fusion* **49** 075034
[8] Briguglio S. *et al* 1995 *Phys. Plasmas* **2** 3711
[9] Wang X. *et al* 2011 *Phys. Plasmas* **18** 052504
[10] Wang X. *et al* Kinetic thermal ions effects on Alfvénic fluctuations in tokamak plasmas, THW/2-4Ra
[11] Pizzuto A. *et al* 2010 *Nucl. Fusion* **50** 95005
[12] Crisanti F. *et al* Scenario development for FAST in the view of ITER and DEMO, FTP/2-4
[13] Cardinali A. *et al* Energetic particle physics in FAST H-mode scenario with combined NNBI and ICRH, THW/P7-04
[14] Baiocchi B. *et al* 2011 Physics based modelling of H-mode and advanced tokamak scenarios for FAST: analysis of the role of rotation in predicting core transport in future machine *Nucl. Fusion* submitted
[15] Romanelli M. *et al* 2007 *Phys. Plasmas* **14** 082305
[16] Kotschenreuther M. *et al* 1995 *Comput. Phys. Commun.* **88** 128
[17] Canton A. *et al* 2006 *Appl. Opt.* **45** 910
[18] Cesario R. *et al* 2010 *Nature Commun.* http://dx.doi.org/10.1038/ncomms1052
[19] Mailloux J. *et al* 2009 'LH wave absorption and current drive studies by application of modulated LHCD at JET *Proc. 36th Conf. on Controlled Fusion and Plasma Physics (Sofia, Bulgaria, 2009)* vol 33E (ECA) P-5.164 http://epsppd.epfl.ch/Sofia/pdf/P5_164.pdf
[20] Wallace G. *et al* 2010 *Phys. Plasmas* **17** 082508
[21] Cesario R. *et al* 2011 *Plasma Phys. Control. Fusion* **53** 085011
[22] Cesario R. *et al* 2004 *Phys. Rev. Lett.* **92** 175002
[23] Pericoli-Ridolfini V. *et al* 2010 LHCD efficiency and scattering by density fluctuations at the plasma edge *37th Conf. on Controlled Fusion and Plasma Physics (Dublin, Ireland, 2010)* vol 34A (ECA) P5.176 http://epsppd.epfl.ch/Dublin/pdf/P5_176.pdf
[24] Pericoli-Ridolfini V. *et al* 2010 Lower hybrid current drive efficiency in tokamaks and wave scattering by density fluctuations at the plasma edge *Plasma Phys. Control. Fusion* submitted
[25] Sauter O. *et al* 2002 *Phys. Rev. Lett.* **88** 105001
[26] Nowak S. *et al* 2005 *Proc. 32nd Conf. on Controlled Fusion and Plasma Physics* vol 29C (ECA) P-4.034
[27] Esposito B. *et al* 2009 *Phys. Rev. Lett.* **100** 045006
[28] Pericoli-Ridolfini V. *et al* 2007 *Nucl. Fusion* **47** S608
[29] Esposito B. *et al* 2009 *Nucl. Fusion* **49** 065014

[30] Nowak S. and Orefice A. 1994 *Phys. Plasmas* **1** 1242
[31] Anderson D. and Lisak M. 1984 *Phys. Fluids* **27** 2477–82
[32] Angioni C. *et al* 2007 *Nucl. Fusion* **47** 1326
[33] Tudisco O. *et al* 2010 Peaked density profiles and MHD activity on FTU in lithium dominated discharges *Fusion Eng. Des.* **85** 902–9
[34] Zonca F. *et al* 2007 *Nucl. Fusion* **47** 1588
[35] Zonca F. et al 2009 Nucl. Fusion 49 085009
[36] Milovanov A.V. 2010 *Europhys. Lett.* **89** 60004
[37] Cardinali A. and Zonca F. 2003 *Phys. Plasmas* **10** 4199
[38] Cardinali A. *et al* 2007 *Phys. Plasmas* **14** 112506
[39] Chen L. 1994 *Phys. Plasmas* **1** 1519
[40] Guimaraes-Filho Z.O. *et al* 2009 Evolution of the electron fishbone-like mode localisation during frequency jumps on Tore Supra *11th IAEA Technical Meeting on Energetic Particles in Magnetic Confinement Systems (Kyiv, Ukraine, 2009)* P10 http://www.kinr.kiev.ua/TCM/posters.htm
[41] White R.B. *et al* 1983 *Phys. Fluids* **26** 2958
[42] Chen L., White R.B. and Rosenbluth M.N. 1984 *Phys. Rev. Lett.* **52** 1122
[43] Zonca F. *et al* 2005 *Nucl. Fusion* **45** 477
[44] Zonca F. *et al* 2007 Electron fishbones: theory and experimental evidence http://arxiv.org/abs/0707.2852v1 [physics.plasm-ph]
[45] Heidbrink W.W. 1993 *Phys. Rev. Lett.* **71** 895
[46] Buratti P. *et al* 2005 *Nucl. Fusion* **45** 1446
[47] Zimmermann O. *et al* 2005 Coupling of Alfvén-like modes and large 2/1 tearing modes at TEXTOR *Proc. 32nd EPS Conf. on Plasma Physics (Tarragona, Spain, 2005)* vol 29C (ECA) P4.059 http://epsppd.epfl.ch/Tarragona/pdf/P4_059.pdf
[48] Garcia-Munoz M. *et al* 2008 *Phys. Rev. Lett.* **100** 055005
[49] Nguyen C. *et al* 2009 *Plasma Phys. Control. Fusion* **51** 095002
[50] Chen W. *et al* 2011 *Nucl. Fusion* **51** 063010
[51] Chen L. and Zonca F. 2007 *Nucl. Fusion* **47** S727
[52] Zonca F. 2008 *Int. J. Mod. Phys.* A **23** 1165
[53] Zonca F. *et al* 2006 *Plasma Phys. Control. Fusion* **48** B15
[54] Zonca F. and Chen L. 2006 *Plasma Phys. Control. Fusion* **48** 537
[55] Zonca F. and Chen L. 2007 The general fishbone-like dispersion relation: a unified description for shear Alfvén mode excitations *Proc. 34th EPS Conf. on Plasma Physics (Warsaw, Poland, 2–6 July 2007)* vol 31F (ECA) CD-ROM file P4.071 http://epsppd.epfl.ch/Warsaw/pdf/P4_071.pdf
[56] Zonca F. *et al* 1996 *Plasma Phys. Control. Fusion* **38** 2011
[57] Chavdarovski I. and Zonca F. 2009 *Plasma Phys. Control. Fusion* **51** 115001
[58] Lauber Ph. *et al* 2009 *Plasma Phys. Control. Fusion* **51** 124009
[59] Zonca F. *et al* 2010 Kinetic structures of shear Alfvén and acoustic wave spectra in burning plasmas *J. Phys.: Conf. Ser.* **260** 012022
[60] Botrugno A. *et al* 2010 Comparison between BAE observations at FTU and theoretical models *37th Conf. on Controlled Fusion and Plasma Physics (Dublin, Ireland, 2010)* vol 34A (ECA) P4.110 http://epsppd.epfl.ch/Dublin/pdf/P4_110.pdf
[61] Annibaldi S.V. *et al* 2007 *Plasma Phys. Control. Fusion* **49** 475
[62] Biancalani A. *et al* 2010 Continuous spectrum of shear Alfvén waves inside magnetic islands *37th Conf. on Controlled Fusion and Plasma Physics (Dublin, Ireland, 2010)* vol 34A (ECA) P4.109 http://epsppd.epfl.ch/Dublin/pdf/P4_109.pdf
[63] Biancalani A. *et al* 2010 *Phys. Rev. Lett.* **105** 095002
[64] Briguglio S. *et al* 1998 *Phys. Plasmas* **5** 3287
[65] Wang X. *et al* 2010 *Plasma Phys. Control. Fusion* **52** 115005
[66] Deng W. *et al* 2010 Gyrokinetic particle simulations of reversed shear Alfvén eigenmode excited by antenna and fast ions *Phys. Plasmas* **17** 112504
[67] Vlad G. *et al* 2009 Toward a new hybrid MHD gyrokinetic code: progresses and perspectives *11th IAEA Technical Meeting on Energetic Particles in Magnetic Confinement Systems (Kyiv, Ukraine, 21–23 September 2009)* p P-25 http://www.kinr.kiev.ua/TCM/posters.htm
[68] Vlad G. *et al* 2010 Hybrid MHD-gyrokinetic codes for studying the mutual nonlinear interaction of shear Alfvén modes and energetic particles *Annual Meeting of the Integrated Tokamak Modelling Task Force, EFDA (Lisbon, Portugal, 13–15 September 2010)* https://www.efda-itm.eu/ITM/imports/imp5/public/meetings/20100913-17_Lisbon/Talk_Vlad_HMGC_HYMAGYC_ITM_GM2010.pdf
[69] Luetjens H. *et al* 1992 *Phys. Commun.* **69** 287
[70] Bondeson A. *et al* 1992 Computation of resistive instabilities in toroidal plasmas *Proc. IAEA Technical Committee Meeting on Advances in Simulation and Modelling of Thermonuclear Plasmas (Montreal, Canada, 1992)* pp 306-15